Spin-selective currents of Tamm polaritons

Evgeny Sedov,[1, 2, 3, 4, *] Mikhail Glazov,[5] and Alexey Kavokin[1, 2, 4, 6]

[1] *Key Laboratory for Quantum Materials of Zhejiang Province, School of Science, Westlake University, 18 Shilongshan Road, Hangzhou 310024, Zhejiang Province, China*
[2] *Institute of Natural Sciences, Westlake Institute for Advanced Study, 18 Shilongshan Road, Hangzhou 310024, Zhejiang Province, China*
[3] *Vladimir State University named after A. G. and N. G. Stoletovs, 87 Gorky str., Vladimir 600000, Russia*
[4] *Spin Optics laboratory, St-Petersburg State University, 1 Ulyanovskaya, St. Petersburg 198504, Russia*
[5] *Ioffe Institute, 26 Polytechnicheskaya, St. Petersburg 194021, Russia*
[6] *School of Physics and Astronomy, University of Southampton, Highfield, Southampton SO171BJ, United Kingdom*

We propose an approach to the excitation of polariton Tamm states with a controllable non-trivial topology. The Tamm polaritons emerge at the interface of two binary one-dimensional photonic crystals belonging to a C_{3v} point group, with an exciton resonance within their matching band gaps. The external magnetic field applied in the Faraday geometry endows the dispersion of the Tamm polaritons with the non-reciprocity: It lifts the degeneracy between opposite propagation directions in the interface plane. The phenomenology of Tamm polariton currents closely resembles one of a Z_2 topological insulator. The proposed structure acts as an optical spin-splitter controlled by the magnetic field magnitude.

I. INTRODUCTION

Engineering of energy bands for light in semiconductor heterostructures forms the basis of topological photonics [1, 2]. Combining optical structures with different energy band structures one can trigger formation of non-trivial topological objects, namely, surface modes, appearing due to the bulk-edge correspondence [3, 4]. In photonics, among such objects are, e. g., surface plasmons emerging at the boundary of a metal and a dielectric [5], optical Tamm states at the interface of two stratified dielectric media [6], and Tamm plasmons at the boundary between a metal and a dielectric Bragg mirror [7, 8]. Optical Tamm states are in the focus of our consideration in this paper. They emerge at the interface between two layered photonic structures with overlapping band gaps [6, 9]. Such states are topologically protected, in a sense that they are stable against variation of the thicknesses of the layers of the structure in which they arise [10].

The strong light-matter coupling regime and the use of active media which willingly respond to the external impact, electric and magnetic fields, allow one to effectively control optical properties of the whole system multilayer system. One of the approaches to achieve the strong coupling regime is embedding quantum wells in all layers of the same refractive index in the structure [11–13]. An alternative approach consists in using bulk materials characterised with an exciton resonance whose energy matches the energy of an optical mode under study [14]. Exciton-polariton modes (polariton modes for brevity) emerge in such structures in the strong light-matter coupling regime [15].

The peculiar property of stratified media is the splitting of the transverse electric (TE or s) and transverse magnetic (TM or p) modes [16, 17]. A monotonic increase of its magnitude with the squared in-plane wave vector k^2 for photons is replaced with a more complex dependence for polaritons. The splitting is azimuthally anisotropic and varies with the double azimuth angle. Herewith it does not break the spatial inversion symmetry and keeps the dispersion of the eigenmodes of the structure reciprocal, $\omega(\mathbf{k}) = \omega(-\mathbf{k})$. To introduce spectral nonreciprocity for polariton modes, one can act upon its exciton fraction. It can be done in a controllable way by applying the external fields to the structure.

The non-reciprocal dispersion was demonstrated for optical Tamm states at the interface of two different magnetophotonic crystals [9]. The magnetic field applied in the Voigt geometry breaks the time-reversal symmetry of the system affecting the TM mode and keeping the TE mode unaffected, so the orthogonal linear polarizations remain independent of each other. In the optical microcavity, the spectral symmetry break under a combined effect of perpendicular magnetic and electric fields was reported in [18].

In this work, we demonstrate the possibility of excitation of Tamm polariton states with the spectral nonreciprocity, $\omega(\mathbf{k}) \neq \omega(-\mathbf{k})$, in the presence of an external magnetic field applied in the Faraday geometry. We show that the Tamm resonance in a planar multilayer structure may act as an optical spin-splitter triggered by the magnetic field.

II. DETAILS OF THE STRUCTURE

The structure under consideration is schematically shown in Fig. 1. It is formed of two (top and bot-

* evgeny_sedov@mail.ru

tom) binary stratified media composed of 14 and 7 pairs of layers SiO_2/CdTe. The bottom structure is grown on the SiO_2 substrate along the $z \parallel [111]$. The choice of the materials is justified as follows. First, the layers of CdTe are active media with the exciton resonance at $\omega_X \approx 1.67$ eV. Second, the high refractive index contrast of the materials estimated as $(n_{b0} - n_a)/n_{b0} \approx 0.46$ results in a strong splitting in the TE and TM polarizations. Third, optical properties of CdTe can be effectively controlled via manipulation its dielectric tensor $\hat{\varepsilon}_b$ by the external magnetic field [19]. The bulk CdTe is a cubic semiconductor with T_d point symmetry group. The considered structure with the growth axis z oriented along the [111] crystal axis belongs to the C_{3v} point group which is a prerequisite for the discussed effects. The symmetry of the system allows for the magneto-spatial dispersion resulting in the bi-linear kB-terms in the dielectric permittivity, with $\mathbf{k}$ being the light wave vector and $\mathbf{B}$ being the magnetic field. Accordingly, the dielectric tensor can be expanded as $\hat{\varepsilon}_b = \hat{\varepsilon}_b^{(0,0)} + \hat{\varepsilon}_b^{(0,1)}(\mathbf{B}) + \hat{\varepsilon}_b^{(1,1)}(\mathbf{k},\mathbf{B})$. In the considered geometry, the components of this tensor are found to be [19, 20]:

$$\varepsilon_{b,\alpha\alpha}^{(0,0)} = \varepsilon_{b0}[1 + \omega_{LT}(\omega_X - \omega - i\Gamma)^{-1}], \tag{1a}$$

$$\varepsilon_{b,xy}^{(0,1)} = -\varepsilon_{b,yx}^{(0,1)} = i\gamma_1 B_z, \tag{1b}$$

$$\frac{\varepsilon_{b,xx}^{(1,1)}}{g} = -\frac{\varepsilon_{b,yy}^{(1,1)}}{g} = \frac{\varepsilon_{b,yz}^{(1,1)}}{h} = \frac{\varepsilon_{b,zy}^{(1,1)}}{h} = -k_x B_z, \tag{1c}$$

$$\frac{\varepsilon_{b,xy}^{(1,1)}}{g} = \frac{\varepsilon_{b,xz}^{(1,1)}}{h} = \frac{\varepsilon_{b,yx}^{(1,1)}}{g} = \frac{\varepsilon_{b,zx}^{(1,1)}}{h} = k_y B_z. \tag{1d}$$

The components not indicated in (1) are equal to zero. In (1a) $\alpha = x, y, z$; ε_{b0} is the background dielectric constant, ω_{LT} is the exciton LT splitting frequency, Γ is the nonradiative decay rate. γ_1 characterizes the Zeeman splitting, g and h are responsible for the magneto-spatial dispersion, and k^2 terms in the bulk exciton dispersion are disregarded. A detailed information on the optical properties of CdTe can be found in Appendix A.

The bottom substructure is the Bragg mirror with the polariton resonance at the edge of its first photonic band gap. In the top substructure the Bragg condition is violated so that the second photonic band gap opens. Due to almost twice wider layers of the top substructure, its second band gap overlaps with the first band gap of the bottom substructure.

III. CHARACTERIZATION OF TAMM POLARITON STATES

The condition for the emergence of the Tamm polariton states can be obtained following the approach developed for calculation of Tamm plasmons in [7]. Let us consider two oppositely directed waves propagating from the interface to the top substructure and

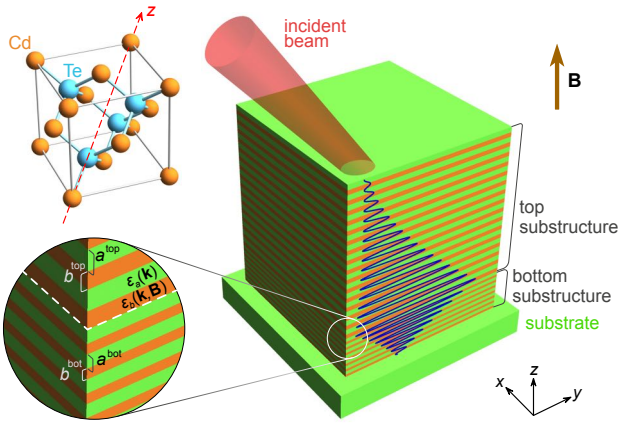

FIG. 1. Schematic of excitation of the Tamm polariton. The external magnetic field $\mathbf{B}$ is applied in the structure growth direction. The inset shows the unit cell of CdTe in the coordinate system considered in the manuscript with $z \parallel [111]$.

to the bottom substructure. Reflection of the corresponding waves is characterized by the amplitude reflection coefficient matrix of the form $\hat{r}_{ij}^L$, where $L = \text{top}, \text{bottom}$, and $i, j = \text{s}, \text{p}$ indicate the polarization of the incident (first index) and reflected (second index) wave at the interface. The diagonal terms, r_{pp}^L and r_{ss}^L, characterize reflection of the wave without the change of its polarization. The magnetic field mixes the polarizations of the waves, so the off-diagonal terms, r_{ps}^L and r_{sp}^L, characterize the rotation of the polarization upon reflection. In order to enable the existence of the Tamm state, the field of a given polarization entering the top (bottom) substructure should match the field of the same polarization reflected from the bottom (top) substructure. The condition for the Tamm polariton state formation takes the following form:

$$(r_{ii}^{\text{top}} r_{ii}^{\text{bot}} + r_{ji}^{\text{top}} r_{ij}^{\text{bot}}) f_p + (r_{jj}^{\text{top}} r_{jj}^{\text{bot}} + r_{ij}^{\text{top}} r_{ji}^{\text{bot}}) f_s = f_i, \tag{2}$$

where $i, j = \text{s}, \text{p}$, and $f_s = \sin\theta$, $f_p = \cos\theta$, with the complex parameter θ that characterizes both the angle of the polarization plane and ellipticity of polarization. See Appendices B–D for details of derivation of Eq. (2). In the absence of the magnetic field ($\mathbf{B} = 0$) the TE and TM polarizations are decoupled and the condition (2) reduces to $r_{ii}^{\text{top}} r_{ii}^{\text{bot}} = 1$, and $r_{ij}^L = 0$.

The dispersion of the doublet of the polariton Tamm states in the cavity plane calculated using the generalized 4×4 transfer matrix method (TMM) [21–24] in the presence of the external magnetic field ($B_z = 10$ T) is shown in Fig. 2(a). Details of TMM are presented in Appendices Appendices B–C. Values of the parameters used in this calculation are given in [25]. The orientation of the dispersion surface is defined by the choice of coordinate axes. We use here

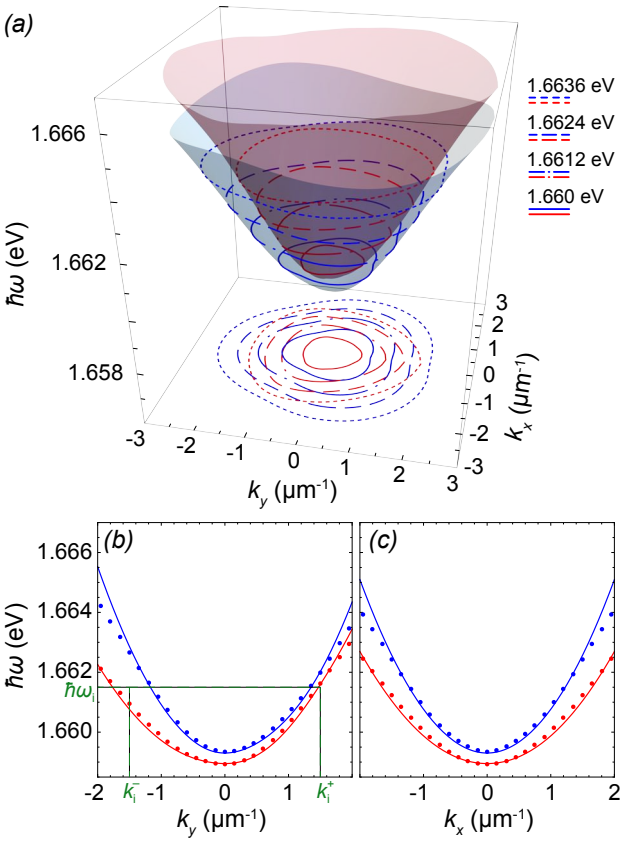

FIG. 2. (a) Dispersion of orthogonally polarized Tamm polariton states at $B_z = 10$ T calculated using TMM. Contours of the same line type correspond to the same energy. (b,c) Dispersions of Tamm states obtained from TMM (dots) and from the Hamiltonian (3) (solid lines) at $k_x = 0$ (b) and $k_y = 0$ (c). Dashed lines in (b) indicate the parameters used for Fig. 3.

the frame with $x \parallel [11\bar{2}]$, $y \parallel [\bar{1}10]$, and $z \parallel [111]$ being the growth axis of the structure (see the inset in Fig. 1). Note that for this choice of axes the three-fold rotation axis $C_3 \parallel z$, and one of three vertical reflection planes is (xz), i.e., the reflection $y \to -y$ is present in the symmetry group of the structure resulting from the magnetic response of the CdTe layers.

The effective 2×2 Hamiltonian for the polariton doublet of the Tamm states can be derived by the method of invariants and takes the form

$$H = \frac{\hbar^2 k^2}{2m^*} + C_1 S_z B_z + C_2[(k_x^2 - k_y^2)S_x + 2k_x k_y S_y] + C_3(k_x S_y + k_y S_x)B_z. \quad (3)$$

The Hamiltonian acts on the spinor $E = [E_+(\mathbf{r}), E_-(\mathbf{r})]^{\mathrm{T}}$ characterizing electric field in the right-circularly, $E_+(\mathbf{r})$, and left-circularly, $E_-(\mathbf{r})$, polarized components. Here we introduced the pseudospin operator $\hat{\mathbf{S}} = (S_x, S_y, S_z)$, with S_α $(\alpha = x, y, z)$ being the 2×2 Pauli matrices, the unit matrix in Eq. (3) is omitted, $\mathbf{k} = (k_x, k_y)$ is the polariton in-plane wave vector. The Hamiltonian is parametrized by four constants: m^* being the effective mass and $C_1, \dots C_3$ are responsible for the effective magnetic fields acting on the polariton pseudospin. The S_z component of the pseudospin is responsible for the circular polarization. It transforms as the z-component of the magnetic field $\mathbf{B}$. The constant C_1 is responsible for the Zeeman splitting, the constant C_2 describes the exciton longitudinal-transverse splitting. The term with C_3 arises in the C_{3v} point symmetry only, it is responsible for the magnetospatial dispersion, see Ref. [26]. In Eq. (3) we take into account the terms up to k^2. See Appendix E for details of derivations of the non-magnetic part of the Hamiltonian.

The effective Hamiltonian (3) can be readily diagonalized as

$$\mathcal{E}_\pm(\mathbf{k}) = \frac{\hbar^2 k^2}{2m^*} \pm \delta_{\mathbf{k}}, \quad (4)$$

where

$$\delta_{\mathbf{k}} = \sqrt{B_z^2(C_3^2 k^2 + C_1^2) + C_2^2 k^4 + 2C_2 C_3 B_z k^3 \sin 3\varphi}. \quad (5)$$

and φ is the angle between the wave vector and x-axis. The eigenenergies (4) are illustrated in Fig. 2(b,c) in comparison with the results of TMM calculations. A good agreement between the TMM and effective Hamiltonian approach is seen, see Ref. [27] for the parameters of Eq. (3). One can readily check that the spectrum at $\mathbf{B} \neq 0$ always has a gap at small k. Indeed, the Hamiltonian can be presented as

$$H = \hbar^2 k^2 / 2m^* + (\boldsymbol{\delta}_{\mathbf{k}} \mathbf{S}), \quad (6)$$

where $\boldsymbol{\delta}_{\mathbf{k}}$ is a vector governed by B_z and $\mathbf{k}$ whose absolute value is given by Eq. (5). To close the gap, $\delta_{\mathbf{k}}$ should turn to zero, which is possible only at $B_z = 0$. In fact, the magnetic field opens a gap in the spectrum of 2D Tamm polaritons.

Depending on the parameters the gap can have a topological nature and, as a result, the system will demonstrate non-trivial one-dimensional edge states. To demonstrate the effect, we derive the Berry curvature

$$\mathcal{F}_{xy}^\pm = \mp \frac{1}{2\delta_{\mathbf{k}}^3} \boldsymbol{\delta}_{\mathbf{k}} \cdot (\partial_{k_x} \boldsymbol{\delta}_{\mathbf{k}} \times \partial_{k_y} \boldsymbol{\delta}_{\mathbf{k}}), \quad (7)$$

where the $\pm$ signs refer to the upper and lower band in Eq. (4), respectively and calculate the Chern numbers as

$$\mathcal{C}^\pm = 2\pi \sum_{\boldsymbol{k}} \mathcal{F}_{xy}^\pm = \mp \int_0^\infty dk k \int_0^{2\pi} \frac{d\varphi}{2\pi} C_1 B_z \frac{C_2 k^2 - (C_3 B_z/2)^2}{4\delta^2}, \quad (8)$$

with the result

$$\mathcal{C}^\pm = \mp \operatorname{sign} C_1 B_z \quad \text{at} \quad C_2 \neq 0. \quad (9)$$

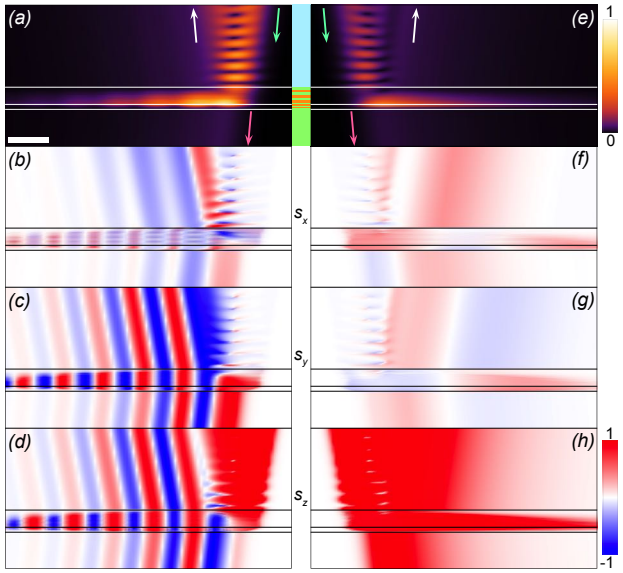

FIG. 3. Polariton Tamm states excited by inclined Gaussian beams with $\hbar\omega_\mathrm{i} = 1.6615$ eV, $k_y = k_\mathrm{i}^- = -1.5\,\mu\mathrm{m}^{-1}$ (a–d) and $k_y = k_\mathrm{i}^+ = 1.5\,\mu\mathrm{m}^{-1}$ (e–h). The width of the beams is $w = 3\,\mu$m. The polarization of the excitation beam is right circular. Green, pink and white arrows in (a) and (e) indicate directions of the incident, transmitted and reflected beams, respectively. The inset between (a) and (e) shows schematically the considered structure. Horizontal lines in each panel indicate the interfaces (from top to bottom) "air–top substructure", "top substructure – bottom substructure" and "bottom substructure – substrate". The white bar in (a) corresponds to $10\,\mu$m

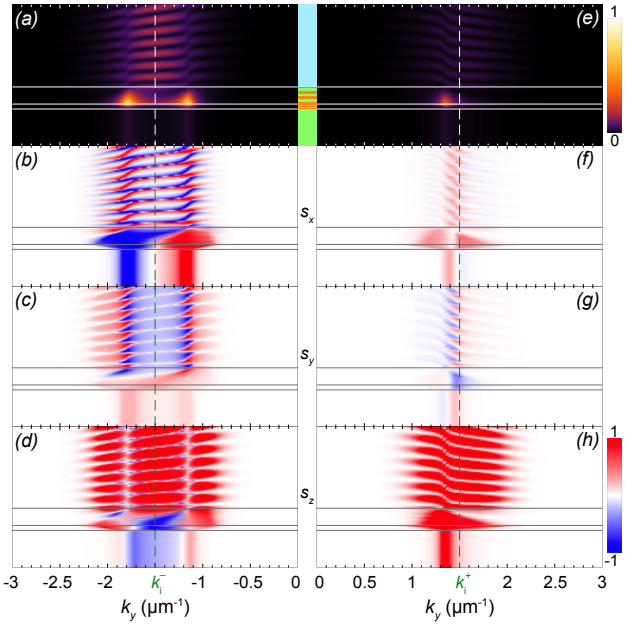

FIG. 4. Distribution in the (k_y, z) plane of the polariton Tamm states shown in Fig. 3. The dashed line indicates the incident beam wave vector $k_y = k_\mathrm{i}^- = -1.5\,\mu\mathrm{m}^{-1}$ (a–d) and $k_y = k_\mathrm{i}^+ = 1.5\,\mu\mathrm{m}^{-1}$ (e–h). The parameters used for calculations are the same as for Fig 3.

Note that at $C_2 = 0$ the Hamiltonian's topological properties are ill-defined, and Eq. (8) gives half-integer Chern numbers [28]. Interestingly, the Chern numbers do not depend on $C_3 \neq 0$ as can be verified by decomposing the sub-integral expression in the series in C_3. The Hamiltonian Eq. (3) at small k is analogous to the Hamiltonian describing electronic states in two-dimensional Z_2 topological insulator.

IV. MAGNETICALLY CONTROLLED TAMM POLARITONS

The non-reciprocity of the spectrum of the Tamm polariton doublet results in its featured intensity and polarization properties. In Fig. 3 we show the distribution of the intensity, $I = E^\dagger E$, and the polarization components, $s_\alpha = (E^\dagger S_\alpha E)/I$ $(\alpha = x, y, z)$, in the plane (y, z) of the polariton states excited by the incident beam of a Gaussian shape $E_\mathrm{i} \propto \exp[-y^2/2w^2]\exp[\mathrm{i}(k_\mathrm{i}^\pm y - \omega_\mathrm{i} t)]$ of width $w = 3\,\mu$m. The energy $\hbar\omega_\mathrm{i}$ and the wave number $k_\mathrm{i}^\pm$ are taken 1.6615 eV and $\pm 1.5\,\mu\mathrm{m}^{-1}$, respectively. The polarization of the incident beam is taken right-circular, $(1, 0)^\mathrm{T}$. The distribution of the spatial spectrum in the structure growth direction is shown in Fig. 4. As one can see in Fig. 2(b), in the case of $k_y = k_\mathrm{i}^+ > 0$ (right panels in Fig. 3) the TE-TM splitting vanishes and the incident beam is close to the resonance with both components of the Tamm polariton doublet. The spectra of the two branches merge and form a single maximum close to the incident wave vector in Fig. 3(e). The incident energy is effectively transferred to the Tamm state localized at the interface of the two substructures. The reflected beam is weakly pronounced, and it is mostly manifested in the formation of the interference fringes in the upper part of Figs. 3(e) and 4(e). The Tamm polariton inherits the circular polarization of the incident beam, see Figs. 3(h) and 4(h).

The Tamm polariton mode propagating in the opposite direction $(k_y = k_\mathrm{i}^- < 0)$ considerably differs from the state discussed above (left panels in Figs. 3 and 4). The center of the spectrum of the incident beam, k_i^-, is far from resonance with both eigenmodes. It is separated from them by more than $0.25\,\mu\mathrm{m}^{-1}$. This results in a much more pronounced reflected beam. Due to the strong TE-TM splitting at the incident energy $\hbar\omega_\mathrm{i}$, the propagation constants of the orthogonally polarized components of the Tamm polariton state along the interface differ from each other by more than $0.5\,\mu\mathrm{m}^{-1}$. One can see two clearly distinguishable maxima in Fig. 4(a) distant from k_i^-. The intensity and the polarization distribution of the emerging Tamm polariton state experience beats in real space. Figure 3(a) shows the intensity distribution of the Tamm state which is periodically mod-

ulated along the propagation direction y. The pure circular polarization of the incident beam, Figs. 3(d), converts to the polarization patterns representing alternating domains of diagonal and circular polarizations of the Tamm polariton state, cf. Figs. 3(g,h) and Figs. 3(c,d). In the reciprocal space, the two lines possess orthogonal linear polarizations, see Fig. 4(b). The period of oscillations of both intensity and polarization distributions is determined by the magnitude of the TE-TM splitting and is about $10\,\mu\text{m}^{-1}$. The formation of alternating polarization patterns due the interference of energy split eigenmodes is the manifestation of the optical spin Hall effect: the phenomenon well known for polaritons in optical microcavities [29–31]. The form of the Hamiltonian (3) indicates the possibility of manifestation in the proposed structure of another polarization-splitting-induced effect known in microcavities, that is the zitterbewegung [32–34]. The effect is expected to manifest itself as oscillations of the trajectory of the Tamm polariton in the interface plane acompanying the oscillations of the polarization.

V. CONCLUSION

We have proposed a resonant optical structure which supports formation of Tamm polariton states with the controllable non-reciprocal dispersion. The Tamm states emerge at the interface of two substructures representing stratifies media belonging to the C_{3v} symmetry group with merging odd and even band gaps. The non-reciprocity of the spectrum emerges under the external magnetic field applied in the Faraday geometry. The magnetospatial dispersion endows the polarization properties of the structure with the non-reciprocity and gives a wide control over the polarization of the Tamm polariton states. We would like to underline that a homogeneous planar multilayer structure discussed here is easy to fabricate, in contrast to two-dimensional patterned structures used for realization of polariton topological insulators in the previous works [35]. The simplicity of design make structures that sustain Tamm modes especially attractive for applications in topological polaritonics.

ACKNOWLEDGEMENTS

A.K. acknowledges the support by Westlake University, Project 041020100118 and Program 2018R01002 funded by Leading Innovative and Entrepreneur Team Introduction Program of Zhejiang Province of China. The Russian Foundation for Basic Research (Grant No. 21-52-10005), Saint-Petersburg State University (Grant No. 91182694), the Grant of the President of the Russian Federation for state support of young Russian scientists (No. MK-4729.2021.1.2) and the Royal Society International Exchange Grant No. IEC/R2/202148 are acknowledged.

Appendix A: Characterization of the materials forming the structure

The structure considered in the manuscript is composed of two SiO_2/CdTe substructures. The SiO_2 layers are considered optically-isotropic, characterized by the dielectric constant $\varepsilon_a = 2.25$. Bulk CdTe is a cubic semiconductor with T_d point symmetry group. The dielectric tensor of CdTe can be represented as following [19, 36, 37]:

$$\hat{\varepsilon}_b = \hat{\varepsilon}_b^{(0,0)} + \hat{\varepsilon}_b^{(0,1)}(\mathbf{B}) + \hat{\varepsilon}_b^{(1,1)}(\mathbf{k},\mathbf{B}). \tag{A1}$$

The first term in the right-hand side of Eq. (A1), $\hat{\varepsilon}_b^{(0,0)}$, corresponds to no magnetic field and spatial dispersion. Its components coincide with (1a) in the rotated frame. The components of the linear in $\mathbf{B}$ term, $\hat{\varepsilon}_b^{(0,1)}(\mathbf{B})$, are given as following:

$$\varepsilon_{b,\alpha\beta}^{(0,1)} = \mathrm{i}\gamma_1\delta_{\alpha\beta\zeta}B_\zeta \quad (\alpha,\beta,\zeta = x,y,z). \tag{A2}$$

Here γ_1 is responsible for the Faraday effect, $\delta_{\alpha\beta\zeta}$ is the Levi-Civita symbol. The components of the bilinear term, $\hat{\varepsilon}_b^{(1,1)}(\mathbf{k},\mathbf{B})$, in Eq. (A1) are given by

$$\varepsilon_{b,\alpha\alpha}^{(1,1)} = \gamma_2(k_{\alpha+1}B_{\alpha+1} - k_{\alpha+2}B_{\alpha+2}), \tag{A3a}$$

$$\varepsilon_{b,\alpha\beta}^{(1,1)} = \gamma_3[\mathbf{B}\times\mathbf{k}]_\zeta. \tag{A3b}$$

The constants γ_2 and γ_3 above describe the magnetospatial dispersion. The cyclic rule is applied in (A3): $\alpha + 3 = \alpha$ $(1,2,3 \to x,y,z)$.

In Eqs. (A1)–(A3) the axes x, y and z are oriented along the crystal axes [100], [010] and [001], respectively. The structure joins the C_{3v} point group when the z axis is oriented in [111] direction. To bring the dielectric tensor $\hat{\varepsilon}_b$ to the new coordinates, we perform the following transformation:

$$\hat{\varepsilon}_b \to \hat{R}\hat{\varepsilon}_b\hat{R}^{-1}, \tag{A4}$$

where $\hat{R} = \hat{R}_Z(a_1)\hat{R}_X(a_2)\hat{R}_Z(a_3)$ is the rotation matrix composed of elemental rotation matrices

$$\hat{R}_Z(a_{1,3}) = \begin{pmatrix} \cos a_{1,3} & -\sin a_{1,3} & 0 \\ \sin a_{1,3} & \cos a_{1,3} & 0 \\ 0 & 0 & 1 \end{pmatrix}, \tag{A5a}$$

$$\hat{R}_X(a_2) = \begin{pmatrix} 1 & 0 & 0 \\ 0 & \cos a_2 & -\sin a_2 \\ 0 & \sin a_2 & \cos a_2 \end{pmatrix}. \tag{A5b}$$

For rotating z from [001] to [111], one should take the following Euler angles: $a_1 = 0$, $a_2 \approx 54.736°$ and $a_3 = 45°$. The vectors transform with respect to $\mathbf{k} \to \hat{R}^{-1}\mathbf{k}$ and $\mathbf{B} \to \hat{R}^{-1}\mathbf{B}$. We keep only the component B_z of the magnetic field in the new coordinates. With that said, in the new axes the components of the dielectric tensor $\hat{\varepsilon}_b$ take the form (1) with $g = (\gamma_2 - 2\gamma_3)/\sqrt{6}$ and $h = (\gamma_2 + \gamma_3)/\sqrt{3}$.

Appendix B: Maxwell's equations

Without loss of generality, we consider the propagation in xz plane assuming $k_y = 0$ in (1). Another propagation plane can be chosen by rotating the tensor $\hat{\varepsilon}_b$ around the z axis. According to the continuity conditions at the interfaces, we get the following expressions for the components of the wave vector in a layer j:

$$k_{xj} = k_{x0} = k_0 q,\ k_{yj} = k_{y0} = 0,\ k_{zj} = k_0 \kappa_j, \quad \text{(B1)}$$

where $\mathbf{k}_0$ is the wave vector of the incident wave, $k_0 = \omega_0/c$, ω_0 is the angular frequency of the wave. For convenience, we have introduced the dimensionless quantities q and κ_j for the in-plane and out-of-plane wave vector components, respectively. The Maxwell's equations in a layer j can be written in matrix form as following [24]:

$$\begin{pmatrix} \varepsilon_{xx} - \kappa_j^2 & \varepsilon_{xy} & \varepsilon_{xz} + q\kappa_j \\ \varepsilon_{yx} & \varepsilon_{yy} - q^2 - \kappa_j^2 & \varepsilon_{yz} \\ \varepsilon_{zx} + q\kappa_j & \varepsilon_{zy} & \varepsilon_{zz} - q^2 \end{pmatrix} \begin{pmatrix} E_x \\ E_y \\ E_z \end{pmatrix} = 0. \quad \text{(B2)}$$

The in-plane wave vector component q is conserved when crossing the interfaces of the layers, and it is determined by inclination of the incident beam. The out-of-plane propagation constant κ_j is different in different layers, and it can be found from the following equation:

$$\begin{vmatrix} \varepsilon_{xx} - \kappa_j^2 & \varepsilon_{xy} & \varepsilon_{xz} + q\kappa_j \\ \varepsilon_{yx} & \varepsilon_{yy} - q^2 - \kappa_j^2 & \varepsilon_{yz} \\ \varepsilon_{zx} + q\kappa_j & \varepsilon_{zy} & \varepsilon_{zz} - q^2 \end{vmatrix} = 0, \quad \text{(B3)}$$

which has four roots in the general case. These roots numbered as κ_{jl} $(l = 1, 2, 3, 4)$ characterize four eigenmodes of the electric field. They represent waves of two orthogonal polarizations (s and p) propagating in forward ($\rightarrow$) and backward ($\leftarrow$) directions. The electric field then is represented in the form of a four-component vector

$$\mathbf{E} = \begin{pmatrix} E^{\mathrm{p}}_{\rightarrow} \\ E^{\mathrm{s}}_{\rightarrow} \\ E^{\mathrm{p}}_{\leftarrow} \\ E^{\mathrm{s}}_{\leftarrow} \end{pmatrix} = \begin{pmatrix} E_1 \\ E_2 \\ E_3 \\ E_4 \end{pmatrix}. \quad \text{(B4)}$$

Appendix C: 4×4 transfer matrix

To examine propagation of light through an anisotropic stratified medium, we use the generalized 4×4 transfer matrix formalism [21, 22] capable for treating optical degeneracies arising in isotropic embedded layers [23, 24]. The electric fields in layers j and $j-1$ are interlinked as following

$$\mathbf{E}_{j-1} = \hat{A}_{j-1}^{-1} \hat{A}_j \hat{P}_j \mathbf{E}_j, \quad \text{(C1)}$$

where $\hat{P}_j$ is the 4×4 propagation matrix with the components determined as $P_{j,ll'} = \delta_{ll'} \exp[-\mathrm{i} k_0 \kappa_{jl} d_j]$. $\delta_{ll'}$ is the Kronecker delta, d_j is the thickness of the jth layer The interaction matrix $\hat{A}_j$ takes the form

$$\hat{A}_j = \begin{pmatrix} a_{j11} & a_{j21} & a_{j31} & a_{j41} \\ a_{j12} & a_{j22} & a_{j32} & a_{j42} \\ b_{j11} & b_{j21} & b_{j31} & b_{j41} \\ b_{j12} & b_{j22} & b_{j32} & b_{j42} \end{pmatrix}, \quad \text{(C2)}$$

where the components are given by [23, 24]

$$a_{j11} = a_{j22} = a_{j42} = -a_{j31} = 1, \quad \text{(C3a)}$$

$$a_{j12} = \begin{cases} 0, & \kappa_{j1} = \kappa_{j2}, \\ \frac{\varepsilon^j_{yz}(\varepsilon^j_{zx} + q\kappa_{j1}) - \varepsilon^j_{yx}(\varepsilon^j_{zz} - q^2)}{(\varepsilon^j_{zz} - q^2)(\varepsilon^j_{yy} - q^2 - \kappa^2_{j1}) - \varepsilon^j_{yz}\varepsilon^j_{zy}}, & \kappa_{j1} \neq \kappa_{j2}, \end{cases} \quad \text{(C3b)}$$

$$a_{j13} = \begin{cases} -\frac{(\varepsilon^j_{zx} + q\kappa_{j1})}{\varepsilon^j_{zz} - q^2}, & \kappa_{j1} = \kappa_{j2}, \\ -\frac{(\varepsilon^j_{zx} + q\kappa_{j1})}{\varepsilon^j_{zz} - q^2} - \frac{\varepsilon^j_{zy}}{\varepsilon^j_{zz} - q^2} a_{12}, & \kappa_{j1} \neq \kappa_{j2}, \end{cases} \quad \text{(C3c)}$$

$$a_{j21} = \begin{cases} 0, & \kappa_{j1} = \kappa_{j2}, \\ \frac{\varepsilon^j_{zy}(\varepsilon^j_{xz} + q\kappa_{j2}) - \varepsilon^j_{xy}(\varepsilon^j_{zz} - q^2)}{(\varepsilon^j_{zz} - q^2)(\varepsilon^j_{xx} - \kappa^2_{j2}) - (\varepsilon^j_{xz} + q\kappa_{j2})(\varepsilon^j_{zx} + q\kappa_{j2})}, & \kappa_{j1} \neq \kappa_{j2}, \end{cases} \quad \text{(C3d)}$$

$$a_{j23} = \begin{cases} -\frac{\varepsilon^j_{zy}}{\varepsilon^j_{zz} - q^2}, & \kappa_{j1} = \kappa_{j2}, \\ -\frac{\varepsilon^j_{zx} + q\kappa_{j2}}{\varepsilon^j_{zz} - q^2} a_{21} - \frac{\varepsilon^j_{zy}}{\varepsilon^j_{zz} - q^2}, & \kappa_{j1} \neq \kappa_{j2}, \end{cases} \quad \text{(C3e)}$$

$$a_{j32} = \begin{cases} 0, & \kappa_{j3} = \kappa_{j4}, \\ \frac{\varepsilon^j_{yx}(\varepsilon^j_{zz} - q^2) - \varepsilon^j_{yz}(\varepsilon^j_{zx} + q\kappa_{j3})}{(\varepsilon^j_{zz} - q^2)(\varepsilon^j_{yy} - q^2 - \kappa^2_{j3}) - \varepsilon^j_{yz}\varepsilon^j_{zy}}, & \kappa_{j3} \neq \kappa_{j4}, \end{cases} \quad \text{(C3f)}$$

$$a_{j33} = \begin{cases} \frac{(\varepsilon^j_{zx} + q\kappa_{j3})}{\varepsilon^j_{zz} - q^2}, & \kappa_{j3} = \kappa_{j4}, \\ \frac{(\varepsilon^j_{zx} + q\kappa_{j3})}{\varepsilon^j_{zz} - q^2} + \frac{\varepsilon^j_{zy}}{\varepsilon^j_{zz} - q^2} a_{32}, & \kappa_{j3} \neq \kappa_{j4}, \end{cases} \quad \text{(C3g)}$$

$$a_{j41} = \begin{cases} 0, & \kappa_{j3} = \kappa_{j4}, \\ \frac{\varepsilon^j_{zy}(\varepsilon^j_{xz} + q\kappa_{j4}) - \varepsilon^j_{xy}(\varepsilon^j_{zz} - q^2)}{(\varepsilon^j_{zz} - q^2)(\varepsilon^j_{xx} - \kappa^2_{j4}) - (\varepsilon^j_{xz} + q\kappa_{j4})(\varepsilon^j_{zx} + q\kappa_{j4})}, & \kappa_{j3} \neq \kappa_{j4}, \end{cases} \quad \text{(C3h)}$$

$$a_{j43} = \begin{cases} -\frac{\varepsilon^j_{zy}}{\varepsilon^j_{zz} - q^2}, & \kappa_{j3} = \kappa_{j4}, \\ -\frac{\varepsilon^j_{zx} + q\kappa_{j4}}{\varepsilon^j_{zz} - q^2} a_{j41} - \frac{\varepsilon^j_{zy}}{\varepsilon^j_{zz} - q^2}, & \kappa_{j3} \neq \kappa_{j4}, \end{cases} \quad \text{(C3i)}$$

$$b_{jl1} = \kappa_{jl} a_{jl1} - q a_{jl3}, \quad \text{(C3j)}$$

$$b_{jl2} = \kappa_{jl} a_{jl2} \quad (l = 1, 2, 3, 4). \quad \text{(C3k)}$$

Different expressions for $a_{jll'}$ for degenerate and non-degenerate propagation constants allow avoiding singularities in the interface matrix $\hat{A}_j$. The vectors $\mathbf{a}_{jl} = (a_{jl1}, a_{jl2}, a_{jl3})$ have to be normalized as $\mathbf{a}_{jl} = \mathbf{a}_{jl}/|\mathbf{a}_{jl}|$. The following equation links the input field E_0 with the field in the jth layer of the structure:

$$\mathbf{E}_0 = \hat{T}\mathbf{E}_j = \hat{A}_0^{-1}\hat{A}_1\hat{P}_1\hat{A}_1^{-1}\hat{A}_2\hat{P}_2 \ldots \hat{A}_{j-1}^{-1}\hat{A}_j\hat{P}_j\mathbf{E}_j. \quad \text{(C4)}$$

Appendix D: The Tamm modes

For pure p- and s-polarized incident waves, the reflection and transmission coefficients are calculated as following:

$$r_{\rm pp} = \left(\frac{E^{\rm p}_{\rm refl}}{E^{\rm p}_{\rm inc}}\right)_{E^{\rm s}_{\rm inc}=0} = \frac{T_{31}T_{22} - T_{32}T_{21}}{T_{11}T_{22} - T_{12}T_{21}}, \quad \text{(D1a)}$$

$$r_{\rm ss} = \left(\frac{E^{\rm s}_{\rm refl}}{E^{\rm s}_{\rm inc}}\right)_{E^{\rm p}_{\rm inc}=0} = \frac{T_{11}T_{42} - T_{41}T_{12}}{T_{11}T_{22} - T_{12}T_{21}}, \quad \text{(D1b)}$$

$$r_{\rm ps} = \left(\frac{E^{\rm s}_{\rm refl}}{E^{\rm p}_{\rm inc}}\right)_{E^{\rm s}_{\rm inc}=0} = \frac{T_{41}T_{22} - T_{42}T_{21}}{T_{11}T_{22} - T_{12}T_{21}}, \quad \text{(D1c)}$$

$$r_{\rm sp} = \left(\frac{E^{\rm p}_{\rm refl}}{E^{\rm s}_{\rm inc}}\right)_{E^{\rm p}_{\rm inc}=0} = \frac{T_{11}T_{32} - T_{31}T_{12}}{T_{11}T_{22} - T_{12}T_{21}}, \quad \text{(D1d)}$$

$$t_{\rm pp} = \left(\frac{E^{\rm p}_{\rm trans}}{E^{\rm p}_{\rm inc}}\right)_{E^{\rm s}_{\rm inc}=0} = \frac{T_{22}}{T_{11}T_{22} - T_{12}T_{21}}, \quad \text{(D1e)}$$

$$t_{\rm ss} = \left(\frac{E^{\rm s}_{\rm trans}}{E^{\rm s}_{\rm inc}}\right)_{E^{\rm p}_{\rm inc}=0} = \frac{T_{11}}{T_{11}T_{22} - T_{12}T_{21}}, \quad \text{(D1f)}$$

$$t_{\rm ps} = \left(\frac{E^{\rm s}_{\rm trans}}{E^{\rm p}_{\rm inc}}\right)_{E^{\rm s}_{\rm inc}=0} = \frac{-T_{21}}{T_{11}T_{22} - T_{12}T_{21}}, \quad \text{(D1g)}$$

$$t_{\rm sp} = \left(\frac{E^{\rm p}_{\rm trans}}{E^{\rm s}_{\rm inc}}\right)_{E^{\rm p}_{\rm inc}=0} = \frac{-T_{12}}{T_{11}T_{22} - T_{12}T_{21}}, \quad \text{(D1h)}$$

where the diagonal terms $r_{\rm ss}$ ($t_{\rm ss}$) and $r_{\rm pp}$ ($t_{\rm pp}$) are the reflection (transmission) coefficients for the TE or s and TM or p modes. The off-diagonal components $r_{\rm ps,sp}$ ($t_{\rm ps,sp}$) describe a partial transfer to an opposite mode on reflection (transmission). $E^{\rm s,p}_{\rm inc,\ refl,\ trans}$ are the incident, reflected from and transmitted through the structure field amplitudes of the corresponding polarizations. Following [38], we should note that in anisotropic structures we have to deal with ordinary (o) and extraordinary (e) modes instead of p and s modes. So, to reflect the physical meaning of the transmission coefficients more pedantically, one should have used the following notations for them: $t_{\rm p(p/o)}$, $t_{\rm s(s/e)}$, $t_{\rm p(s/e)}$, $t_{\rm s(p/o)}$, where p and s in parentheses are for isotropic media while o and e are for anisotropic media [39].

Let us now virtually split the structure into two substructures along the interface of the two Bragg mirrors. The field propagating *from the interface to the bottom mirror* is described as follows:

$$\mathbf{E}^{\rm bot}_{\rm inc} = \begin{pmatrix} E^{\rm p}_{\rightarrow} \\ E^{\rm s}_{\rightarrow} \\ E^{\rm p}_{\leftarrow} \\ E^{\rm s}_{\leftarrow} \end{pmatrix} = \begin{pmatrix} E^{\rm p}_{\rightarrow} \\ E^{\rm s}_{\rightarrow} \\ r^{\rm bot}_{\rm pp}E^{\rm p}_{\rightarrow} + r^{\rm bot}_{\rm sp}E^{\rm s}_{\rightarrow} \\ r^{\rm bot}_{\rm ss}E^{\rm s}_{\rightarrow} + r^{\rm bot}_{\rm ps}E^{\rm p}_{\rightarrow} \end{pmatrix}. \quad \text{(D2)}$$

In the transmitted field in the right-hand side of (D2) we have only transmitted components and no reflected components. The same procedure for the field propagating *from the interface to the top mirror* written in the same basis gives

$$\mathbf{E}^{\rm top}_{\rm inc} = \begin{pmatrix} E^{\rm p}_{\rightarrow} \\ E^{\rm s}_{\rightarrow} \\ E^{\rm p}_{\leftarrow} \\ E^{\rm s}_{\leftarrow} \end{pmatrix} = \begin{pmatrix} r^{\rm top}_{\rm pp}E^{\rm p}_{\leftarrow} + r^{\rm top}_{\rm sp}E^{\rm s}_{\leftarrow} \\ r^{\rm top}_{\rm ss}E^{\rm s}_{\leftarrow} + r^{\rm top}_{\rm ps}E^{\rm p}_{\leftarrow} \\ E^{\rm p}_{\leftarrow} \\ E^{\rm s}_{\leftarrow} \end{pmatrix}. \quad \text{(D3)}$$

We take the field going from top to bottom as $(E^{\rm p}_{\rightarrow}, E^{\rm s}_{\rightarrow}) = (\cos\theta, \sin\theta)$, i.e., we parametrize it with the complex parameter θ which defines polarization (both angle and ellipticity) of the field. For the Tamm state to exist, the field of a given polarization entering the top mirror should match the field of the same polarization reflected from the bottom mirror. And vice versa, the field reflected from the top mirror should match the field entering the bottom mirror. Eliminating the components $E^{\rm p}_{\leftarrow}$ and $E^{\rm s}_{\leftarrow}$ from Eqs. (D2) and (D3), we arrive at the equation for the Tamm state (2) with the variables (ω, θ).

Appendix E: The derivation of the effective Hamiltonian of the Tamm state

Let us consider an optically active exciton in a cubic semiconductor crystal. The three optically active states have a total angular momentum $L = 1$ (the polarization induced by the exciton $\mathbf{P}$ is a vector), therefore, it is convenient to express the effective Hamiltonian in terms of the basis matrices of the angular momentum 1: L_x, L_y, L_z and their combinations. According to the general theory of angular momentum, the set of three matrices $\mathbf{L}$ can be treated as a pseudovector. In the isotropic approximation, the effective Hamiltonian accounting terms with powers of the wave vector $\mathbf{k}$ up to two, has the form

$$\mathcal{A}k^2 + \mathcal{B}(\mathbf{L}\cdot\mathbf{k})^2, \quad \text{(E1)}$$

where $\mathcal{A}$ and $\mathcal{B}$ are parameters. We omit the identity matrix for brevity. It is seen that the energy of the "longitudinal" exciton $E_L = \mathcal{A}k^2$ differs from the energy of the two "transverse" states, $E_T = (\mathcal{A}+\mathcal{B})k^2$, which is easy to see directing $\mathbf{k}$ along the z axis. We should note that in reality the spectrum of longitudinal and transverse excitons differs from these simplest formulas, one should take into account the polariton effects. Herewith, the degeneracy multiplicities are preserved, and the polarization of states is described correctly.

Let us now turn to a two-dimensional (or quasi-two-dimensional) model, assuming that $\mathbf{k} \parallel (xy)$, and dimensional quantization and deformation split off a state polarized along the z axis by a significant energy. In the axial approximation, the effective Hamiltonian is written as

$$H_{\rm ax} = \mathcal{A}k^2 + \mathcal{B}(\mathbf{L}\cdot\mathbf{k})^2 + \mathcal{C}L_z^2, \quad \text{(E2)}$$

where the term with $\mathcal{C}L_z^2$ is the splitting of the triplet into the z-state and the doublet polarized in the (xy) plane.

Assuming $\mathcal{B}k^2 \ll \mathcal{C}$ we can consider the doublet independently from the z-state. We note that

$$(\mathbf{L}\cdot\mathbf{k})^2 = L_x^2k^2 + L_y^2k_y^2 + (L_xL_y + L_yL_x)k_xk_y, \quad \text{(E3)}$$

and use the explicit matrix form of $\mathbf{L}$:

$$L_x^2 = \frac{1}{2}\begin{pmatrix}1&0&1\\0&2&0\\1&0&1\end{pmatrix}, \quad \text{(E4a)}$$

$$L_y^2 = \frac{1}{2}\begin{pmatrix}1&0&-1\\0&2&0\\-1&0&1\end{pmatrix}, \quad \text{(E4b)}$$

$$L_xL_y + L_yL_x = \begin{pmatrix}0&0&-\mathrm{i}\\0&0&0\\\mathrm{i}&0&0\end{pmatrix}. \quad \text{(E4c)}$$

We introduce the pseudospin vector $\mathbf{S} = (S_x, S_y, S_z)$, where $S_{x,y,z}$ are the Pauli matrices and rewrite the Hamiltonian of the doublet in the basis of circular polarizations in the following form:

$$H'_{\mathrm{ax}} = (\mathcal{A}+\mathcal{B})k^2 + \mathcal{B}[(k_x^2 - k_y^2)S_x + 2k_xk_yS_y]. \quad \text{(E5)}$$

[1] L. Lu, J. D. Joannopoulos, and M. Soljačić, Topological photonics, Nature Photonics **8**, 821 (2014).

[2] T. Ozawa, H. M. Price, A. Amo, N. Goldman, M. Hafezi, L. Lu, M. C. Rechtsman, D. Schuster, J. Simon, O. Zilberberg, and I. Carusotto, Topological photonics, Rev. Mod. Phys. **91**, 015006 (2019).

[3] Y. Hatsugai, Chern number and edge states in the integer quantum hall effect, Phys. Rev. Lett. **71**, 3697 (1993).

[4] X.-L. Qi, Y.-S. Wu, and S.-C. Zhang, General theorem relating the bulk topological number to edge states in two-dimensional insulators, Phys. Rev. B **74**, 045125 (2006).

[5] S. Kawata, *Near-Field Optics and Surface Plasmon Polaritons* (Springer, 2001).

[6] A. V. Kavokin, I. A. Shelykh, and G. Malpuech, Lossless interface modes at the boundary between two periodic dielectric structures, Phys. Rev. B **72**, 233102 (2005).

[7] M. Kaliteevski, I. Iorsh, S. Brand, R. A. Abram, J. M. Chamberlain, A. V. Kavokin, and I. A. Shelykh, Tamm plasmon-polaritons: Possible electromagnetic states at the interface of a metal and a dielectric bragg mirror, Phys. Rev. B **76**, 165415 (2007).

[8] I. Y. Chestnov, E. S. Sedov, S. V. Kutrovskaya, A. O. Kucherik, S. M. Arakelian, and A. V. Kavokin, One-dimensional tamm plasmons: Spatial confinement, propagation, and polarization properties, Phys. Rev. B **96**, 245309 (2017).

[9] H. Y. Dong, J. Wang, and K. H. Fung, One-way optical tunneling induced by nonreciprocal dispersion of tamm states in magnetophotonic crystals, Opt. Lett. **38**, 5232 (2013).

[10] A. Palatnik, M. Sudzius, S. Meister, and K. Leo, One-dimensional planar topological laser, Nanophotonics **10**, 2459 (2021).

[11] A. Askitopoulos, L. Mouchliadis, I. Iorsh, G. Christmann, J. J. Baumberg, M. A. Kaliteevski, Z. Hatzopoulos, and P. G. Savvidis, Bragg polaritons: Strong coupling and amplification in an unfolded microcavity, Phys. Rev. Lett. **106**, 076401 (2011).

[12] E. S. Sedov, I. V. Iorsh, S. M. Arakelian, A. P. Alodjants, and A. Kavokin, Hyperbolic metamaterials with bragg polaritons, Phys. Rev. Lett. **114**, 237402 (2015).

[13] E. S. Sedov, E. D. Cherotchenko, S. M. Arakelian, and A. V. Kavokin, Light propagation in tunable exciton-polariton one-dimensional photonic crystals, Phys. Rev. B **94**, 125309 (2016).

[14] F. Biancalana, L. Mouchliadis, C. Creatore, S. Osborne, and W. Langbein, Microcavity polaritonlike dispersion doublet in resonant bragg gratings, Phys. Rev. B **80**, 121306 (2009).

[15] A. Kavokin, J. Baumberg, G. Malpuech, and F. Laussy, *Microcavities*, 2nd ed., Series on Semiconductor Science and Technology (OUP Oxford, 2017).

[16] G. Panzarini, L. C. Andreani, A. Armitage, D. Baxter, M. S. Skolnick, V. N. Astratov, J. S. Roberts, A. V. Kavokin, M. R. Vladimirova, and M. A. Kaliteevski, Exciton-light coupling in single and coupled semiconductor microcavities: Polariton dispersion and polarization splitting, Phys. Rev. B **59**, 5082 (1999).

[17] D. Schmidt, B. Berger, M. Bayer, C. Schneider, M. Kamp, S. Höfling, E. Sedov, A. Kavokin, and M. Aßmann, Dynamics of the optical spin hall effect, Phys. Rev. B **96**, 075309 (2017).

[18] H.-T. Lim, E. Togan, M. Kroner, J. Miguel-Sanchez, and A. Imamoğlu, Electrically tunable artificial gauge potential for polaritons, Nature Communications **8**, 14540 (2017).

[19] T. Godde, M. M. Glazov, I. A. Akimov, D. R. Yakovlev, H. Mariette, and M. Bayer, Magnetic field induced nutation of exciton-polariton polarization in (cd,zn)te crystals, Phys. Rev. B **88**, 155203 (2013).

[20] O. V. Gogolin, V. A. Tsvetkov, and E. G. Tsitsishvili, Magnetically induced birefringence in cubic crystals, JETP **60**, 593 (1984).

[21] P. Yeh, Electromagnetic propagation in birefringent layered media, J. Opt. Soc. Am. **69**, 742 (1979).

[22] D. W. Berreman, Optics in stratified and anisotropic media: 4 × 4-matrix formulation, J. Opt. Soc. Am. **62**, 502 (1972).

[23] N. C. Passler and A. Paarmann, Generalized 4 × 4 matrix formalism for light propagation in anisotropic stratified media: study of surface phonon polaritons in polar dielectric heterostructures, J. Opt. Soc. Am. B **34**, 2128 (2017).

[24] W. Xu, L. T. Wood, and T. D. Golding, Optical degeneracies in anisotropic layered media: Treatment of singularities in a 4×4 matrix formalism, Phys. Rev. B **61**, 1740 (2000).

[25] We take the following parameters of the layers of the structure. The dielectric constant of SiO_2 is $\varepsilon_a = 2.25$. The background dielectric constant of CdTe is $\varepsilon_{b0} = 7.8$, the LT-splitting is $\hbar\omega_{\rm LT} = 0.14\,$meV, the nonradiative decay rate is $\hbar\Gamma = 0.1\,$meV, the Zeeman splitting constant is $\gamma_1 = 2 \times 10^{-4}\,{\rm T}^{-1}$, the parameters of the magnetospatial dispersion are $g = -8 \times 10^{-4}\,\mu{\rm m\ T}^{-1}$, $h = 4 \times 10^{-3}\,\mu{\rm m\ T}^{-1}$. The thicknesses of the layers are $a^{\rm top} = 148.6\,$nm, $b^{\rm top} = 164.1\,$nm and $a^{\rm bot} = 101.8\,$nm, $b^{\rm bot} = 54.5\,$nm.

[26] L. V. Kotova, V. N. Kats, A. V. Platonov, V. P. Kochereshko, R. André, and L. E. Golub, Magnetospatial dispersion of semiconductor quantum wells, Phys. Rev. B **97**, 125302 (2018).

[27] The parameters in the Hamiltonian (3) are following. The effective mass is $m^* = 3.2 \times 10^{-5} m_0$, where m_0 is the free electron mass, the Zeeman splitting constant is $C_1 = 15\,\mu{\rm eV\ T}^{-1}$, the TE-TM splitting constant is $C_2 = 0.5\,{\rm meV}\mu{\rm m}^2$, the magneto-induced dispersion constant is $C_3 = 30\,\mu{\rm eV}\,\mu{\rm m\ T}^{-1}$.

[28] This situation is similar to the 2D Dirac equation.

[29] A. Kavokin, G. Malpuech, and M. Glazov, Optical spin hall effect, Phys. Rev. Lett. **95**, 136601 (2005).

[30] C. Leyder, M. Romanelli, J. P. Karr, E. Giacobino, T. C. H. Liew, M. M. Glazov, A. V. Kavokin, G. Malpuech, and A. Bramati, Observation of the optical spin hall effect, Nature Physics **3**, 628 (2007).

[31] D. Caputo, E. S. Sedov, D. Ballarini, M. M. Glazov, A. V. Kavokin, and D. Sanvitto, Magnetic control of polariton spin transport, Communications Physics **2**, 165 (2019).

[32] E. S. Sedov, Y. G. Rubo, and A. V. Kavokin, *Zitterbewegung* of exciton-polaritons, Phys. Rev. B **97**, 245312 (2018).

[33] E. S. Sedov, I. E. Sedova, S. M. Arakelian, and A. V. Kavokin, Magnetic control over the zitterbewegung of exciton–polaritons, New Journal of Physics **22**, 083059 (2020).

[34] E. Sedov, I. Sedova, S. Arakelian, and A. Kavokin, Polygonal patterns of confined light, Opt. Lett. **46**, 1836 (2021).

[35] S. Klembt, T. H. Harder, O. A. Egorov, K. Winkler, R. Ge, M. A. Bandres, M. Emmerling, L. Worschech, T. C. H. Liew, M. Segev, C. Schneider, and S. Höfling, Exciton-polariton topological insulator, Nature **562**, 552 (2018).

[36] B. B. Krichevtsov, A. A. Rzhevskii, and H.-J. Weber, Second-order magnetoelectric susceptibility in the optical region of the boracite $co_3b_7o_{13}i$, Phys. Rev. B **61**, 10084 (2000).

[37] B. B. Krichevtsov, R. V. Pisarev, A. A. Rzhevskii, V. N. Gridnev, and H. J. Weber, Magnetically induced spatial dispersion in the cubic magnetic semiconductors cd1-xmnxte, Journal of Experimental and Theoretical Physics **87**, 553 (1998).

[38] N. C. Passler and A. Paarmann, Generalized 4×4 matrix formalism for light propagation in anisotropic stratified media: study of surface phonon polaritons in polar dielectric heterostructures: erratum, J. Opt. Soc. Am. B **36**, 3246 (2019).

[39] N. C. Passler, M. Jeannin, and A. Paarmann, Layer-resolved absorption of light in arbitrarily anisotropic heterostructures, Phys. Rev. B **101**, 165425 (2020).